

IDEALIZATION OF BOND STRESS-SLIP RELATIONSHIP AT ELEVATED TEMPERATURES BASED ON PULLOUT TESTS

Mohammad Mahdi RAOUF-FARD, M.Sc. Second year,

Masanobu SAKASHITA, Ph.D., Assist. Professor,

Minehiro NISHIYAMA, Ph.D., Professor,

Dept. of Architecture & Architectural Engineering, Kyoto University, Japan

ABSTRACT

Bond stress-slip relationship at elevated temperatures is of great importance for estimating deflections at reinforced concrete (RC) beams and development length for prestressing steel in pretensioned members. However, still little research can be found in literatures on bond performance at elevated temperatures. In an attempt to provide an efficient formulation for bond stress-slip relationship in fire condition for steel reinforcing in RC members, an extensive experimental and analytical study consisted of two series of twenty-one rebar pullout tests of 150×300mm concrete cylinder specimens was carried out. Experiment parameters were concrete strength (24.0 and 36.9MPa) and temperature. Three of the specimens underwent the tests in room temperature and the rest, which were grouped in six sets underwent the tests in 100, 200, 300, 400, 500, and 600°C temperatures at the rate of 3°C/min, respectively. Based on the results, the *fib* Model Code bond stress-slip relationship at room temperature was idealized to a set of formulations at elevated temperatures. The formulations will be implemented in a finite element (FE) modelling software to predict structural performance of RC members and evaluate anchorage performance of steel reinforcing in pretensioned members at elevated temperature.

Keywords: Elevated temperatures, Fire test, Reinforced concrete, Pre-tensioned members, *fib* Model Code, Bond stress-slip relationship, FE modeling

INTRODUCTION

Concrete has considerably lower thermal conductivity than steel and thus is a thermal barrier for embedded reinforcing steel bar, however, the two materials themselves suffer a progressive loss of stiffness and strength with increase of temperature and similarly, bond strength decreases even in a greater extent. Bond is the term of the load-carrying mechanism at the interface of concrete and reinforcement in the longitudinal direction of the reinforcing bar. Sufficient bond strength is essential if a member is to give a satisfactory structural performance, including failure with adequate warning, rather than sudden collapse. In a series of the fire tests on RC frames conducted by the authors^{1, 2}, the influence of bond strength degradation on RC beams' excessive deflections was speculated. Implementing the bond condition at elevated temperatures in numerical and analytical studies requires a series of reduction factor models, of which the bond reduction factor plays a significant role in estimating deflection of fire-exposed RC members, and evaluating of steel reinforcement anchorage development in pretensioned members and so on. To date several extensive experimental and analytical research on bond problem at ambient temperature have been carried out and a variety of models by Rehm³ (1961), Martin⁴ (1973), Harajali⁵ (2006), and Wu⁶ (2013) and so on have been introduced. However, regarding to bond problem at elevated temperatures, yet comparatively a few experimental and numerical works have been done.

In order to study the bond problem in fire, the authors manufactured two series of twenty-one test specimens (series I and II), compatible for pull-out test and heating. The purpose was reproducing bond temperature-dependent formulations based on *fib* Model Code⁷ (2010) in the first place, which is discussed later in this paper. Based on the results of series I, a temperature-dependent bond-slip model was introduced. However, the proposed model is still limited to the test conditions. In the second step, the test specimens of series II ($f_c=36.9\text{MPa}$) were tested similar to the first series. In this step, the effect of concrete strength on bond characteristics such as bond stiffness and strength at elevated temperatures were investigated. Uncertainties such as extent of dominance of concrete and steel strengths on the bond problem of the specimens at high temperatures, yet remained unconfirmed. To approach these uncertainties, in the third step, a series of 2D and 3D FE models have been provided and currently the results of the tests are being regulated and implemented in the FE models to achieve the best-fit approaches to bond problem in fire condition. In this paper, the experiment work and the results are discussed. The details of the numerical study will be published elsewhere.

BOND STRESS-SLIP RELATIONSHIP

Steel-to-concrete bond is the many-faceted phenomenon which allows longitudinal forces to be transferred from the reinforcement to the surrounding concrete in a RC or prestressed concrete structure. Due to this force transfer, the force in a reinforcing bar changes along the length, as does the force in the concrete embedment. Wherever steel strains differ from concrete strains a relative displacement between the steel and the concrete (slip) does occur⁷. For the bond stress-slip relationship the equilibrium and compatibility must be satisfied. **Fig. 1** shows a schematic stress distribution in a reinforcing bar with its peripheral concrete. **Eq. 1** and **2** imply the force equilibrium at bond interface and general equation of bond stress, respectively.

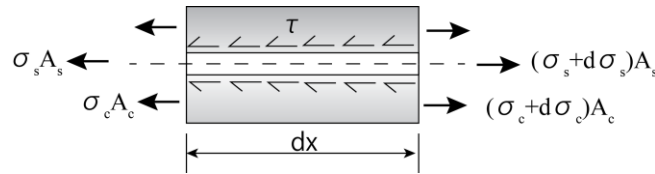


Fig. 1 Stress diagram in reinforcement and concrete

$$A_s d\sigma_s + A_c d\sigma_c = 0 \tag{Eq.(1)}$$

$$\tau = \frac{A_s d\sigma_s}{d_b \pi dx} \tag{Eq.(2)}$$

Where d_b is the bar diameter. A_c and A_s are the cross-sectional areas of the concrete and the bar, σ_c and σ_s are the stresses in concrete and steel, respectively. The increment of the local slip s_x (**Eq. 3**) within an infinitesimal bar length dx at the location of x can be defined as the difference between the extension of the bar, s_s , and the concrete extension, s_c at x .

$$s_x = s_s - s_c \tag{Eq. (3)}$$

Many studies have been made to get a best-fit curve for bond stress-slip relationship from the above equations. However, different initial assumptions between the bond stress and the slip have led to a variety of models. At elevated temperatures thermal induced strains and reduction in material properties and so on even add more complexity to bond problem. For the purpose of this paper the *fib* Code Model 2010⁸ (hereafter *fib* Model) was employed to reproduce idealized bond stress-slip equations at elevated temperatures for the test results. The bond stress-slip relationship introduced by *fib* Model is summarized in the following

equations:

$$\tau = \tau_{\max} \left(s / s_1 \right)^\alpha \quad 0 \leq s \leq s_1 \quad \text{Eq. (4)}$$

$$\tau = \tau_{\max} \quad s_1 \leq s \leq s_2 \quad \text{Eq. (5)}$$

$$\tau = \tau_{\max} - \left(\tau_{\max} - \tau_f \right) \left(\frac{s - s_2}{s_3 - s_2} \right) \quad s_2 \leq s \leq s_3 \quad \text{Eq. (6)}$$

$$\tau = \tau_f \quad s_3 \leq s \quad \text{Eq. (7)}$$

where τ and s are the average bond stress and slip, respectively. The parameters s_1 , s_2 , s_3 , and α are defined in **Table 1**. In order to consider the influence of concrete compressive strength on the average bond stress, the maximum bond stress, τ_{\max} , is directly related to the square root of compressive strength of the concrete. The bond stress-slip curve, represented by the above equations can be considered as a statistical mean curve, applicable as an average formulation for a broad range of cases. The *fib* Model curve is presented in **Fig. 2**. The curve is divided into four stages. In the ascending branch (**Eq. 4**), chemical adhesion breaks down at low bond-stress values ($0.2 \sim 0.8$ concrete splitting tensile strength (f_{ct}))⁷ and for higher bond stresses the lugs induce large bearing stresses in the concrete cause local crushing and transverse micro-cracking at the tip of the lugs allowing bar to slip. Still for higher bond stress values ($1 \sim 3 f_{ct}$)⁷ the longitudinal cracks spread radially, owing to the wedging action. At increasing slip values, the bond strength reaches a peak and then starts decreasing. If enough lateral confinement is provided, the transition to the descending phase is happening at larger slips (**Eq. 5**). The descending branch (**Eq. 6**) represents the dry-friction bond behavior. In this level the concrete between the lugs are crushed or sheared off and the last leveled-off stage (**Eq. 7**) represents the residual bond capacity.

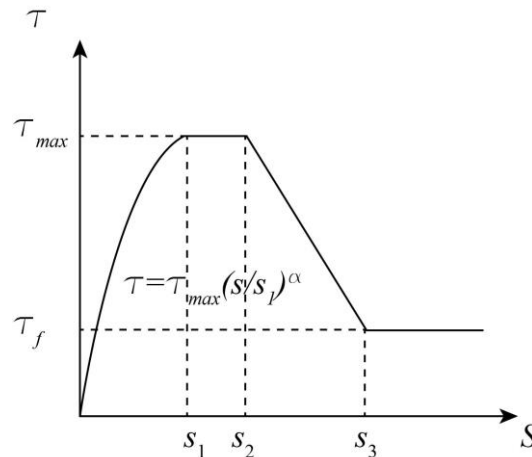


Fig. 2 Bond stress–slip curve defined by CEB-FIP Model Code 2010⁸

Table 1 Parameters of *fib* Model for bond stress-slip relationship⁸

Bond conditions	Unconfined concrete		Confined concrete	
	Good	All other	Good	All other
s_1	0.6mm		1.0mm	
s_2			3.0mm	
s_3	1.0mm	2.5mm	Clear rib spacing	
α	0.4		0.4	
τ_{max} (MPa)	$2.0(f'_c)^{1/2}$	$1.0(f'_c)^{1/2}$	$2.5(f'_c)^{1/2}$	$1.25(f'_c)^{1/2}$
τ_f (MPa)	$0.15\tau_{max}$		$0.40\tau_{max}$	

Bond problem at elevated temperatures is still in its infancy stages. Bazant and Kaplan⁹ (1992) summarized various test results on bond strength degradation factors of smooth and deformed bars in fire condition and according to this study it can be concluded that (a) bond strength decreases as temperature increases and the reduction rate is larger compared to concrete strengths, (b) the bond strength of ribbed steel bars at elevated temperatures is larger than plain round steel bars, (c) the bars diameters have little effect on the bond strength reduction, (d) the type of aggregate affects the bond strength in fire condition, and (e) the smaller the concrete cover is, the larger bond strength reduction is expected¹⁰. Based on this study, Huang¹⁰ (2010) derived simplified bi-linear and tri-linear models and conducted a series of finite element analyses to simulate the bond characteristics of ribbed and smooth bars at elevated temperatures. Later in the test results section, the Huang model is introduced.

EXPERIMENT WORK

SPECIMEN FABRICATION

The test specimens were built according to experiment work by Matsuyoshi et al.¹¹ (2005) on FRP pullout test. Fig. 3 shows the details of the test specimen. As can be seen in the figure, it is a combination of a 150×300mm concrete cylinder, a 1160mm long ϕ 19mm ribbed longitudinal reinforcing bar, and a ϕ 6mm spiral hoop. Twenty-one test specimens were built in two series (series I and II) and in each series, the specimens were divided into seven groups, subjected to heat cycles 18, 100, 200, 300, 400, 500, and 600°C, respectively. The

deformed steel bar inside each concrete cylinder was aligned to the center line of the cylinder. The upper and the lower bar extensions, which were sticking out from the center of both faces of the cylinders were 100mm long (free end) and 760mm long (loaded end), respectively. The reinforcing lug of the bar was 1.5mm high in average and the average spacing between each of the two lugs was 10.4mm. A supplementary deformed steel reinforcement of 6mm diameter provided enough confinement to prevent any possible concrete premature break-up during the bar tensioning. 76mm of the 300mm embedment bar was employed as the bond length (colored in red in **Fig. 3**) according to JCI pullout test recommendations¹² and the two remaining 112mm embedded lengths were shielded with an aluminum casing to act as bond-breakers. Inside each casing was filled with ceramic blanket to lessen heat escape from the bond length during the pullout test (**Fig. 4a**). The steel bars were instrumented with one strain gauge at the length of 250mm from the loaded end and three thermocouples on the confined length; one for each encased length and one for the bond length. Two displacement transducers were later mounted on the top faces of the concrete cylinders (**Fig.7**) to measure the upper free end displacement.

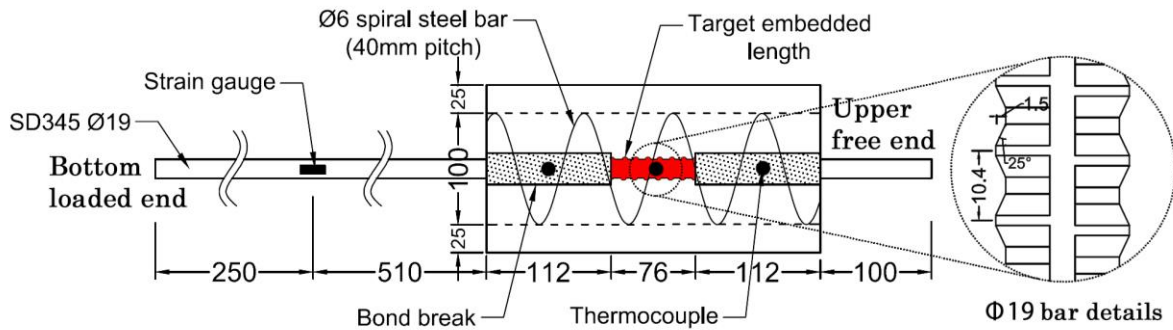


Fig.3 Test specimen geometry (unit: mm)



(a) Rebar preparation



(b) Specimen mold



(c) Concrete casting

Fig. 4 Test specimen preparation

All the specimens were casted with normal-weight concrete. The concrete mixture and the mechanical properties of the concrete and the steel are shown in **Table 2** and **3**. The fabrication process of the test specimens are shown in **Fig. 4a** to **5c**. The specimens were removed from their molds after a week and were cured until the moment of the test.

Table 2 Concrete mix proportion and mechanical properties

Series	Mix portion (kg/m ³)				W/C (%)	Water content (%)	Comp. strength (MPa)	Elastic modulus (GPa)	
	Cement	Water	Aggregate* ¹						Admixture
			fine	coarse					
I	292	184	788	991	2.92	63	5.50	24.0	24.1
II	386	180	538	910	2.90	52	5.44	36.9	22.6

*¹Maximum size = 2 cm

Table 3 Mechanical properties of the steel deformed bar

Series	Type	Nominal section area (mm ²)	Yielding strength (N/mm ²)	Tensile Strength (N/mm ²)	Young's Modulus (×10 ⁵ N/mm ²)
I	D19 SD345	286.5	383	504	1.92
II	D19 SD345	286.5	377	564	1.92

HEATING APPARATUS

Fig. 5 shows the heating mantel used in the heating phase. The heater was wrapped around the concrete cylinder like a jacket and its two caps covered the bottom and the top faces of the concrete cylinder. The heating elements (electric wires) were embedded within a strip of fabric inside the heater. AC 200V current was supplied to the device and hence, the desired temperatures were achieved by regulating a rheostat.

TEST PROCESS

Fig. 6 shows the placement of the specimen and the heating mantel on a 500kN universal

hydraulic test machine. The test process is schematically illustrated in **Fig. 7**.

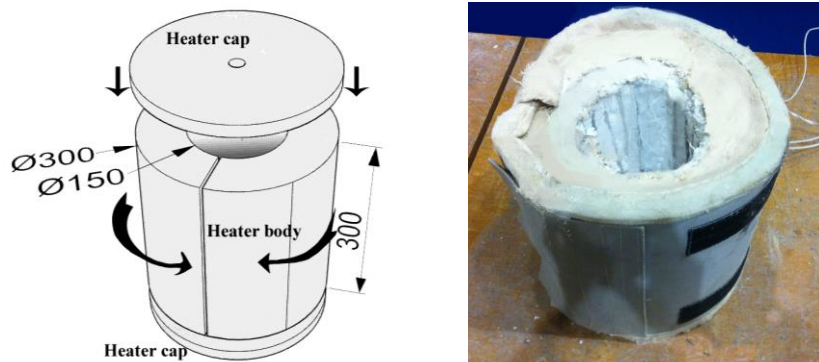


Fig. 5 Heating mantel

According to the **Ref.13** (Ichise et al.) if the heat rate is set between 2.5 to 7.5°C/min, the decreasing effect of rising heat rate on compressive concrete strength is very small and negligible. Hence, in the heating phase (**Fig. 7a**), the concrete cylinder was heated at rate of 3°C/min until the thermocouple on the bond segment reached the target temperature.

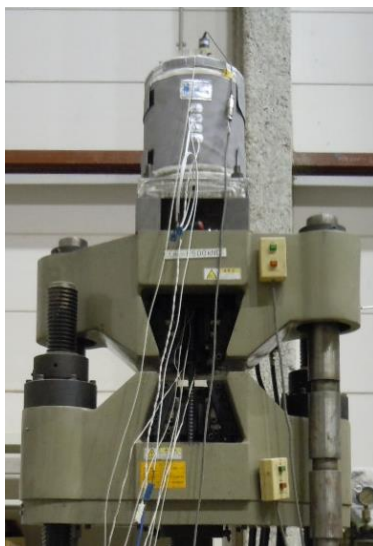


Fig. 6 Test setup

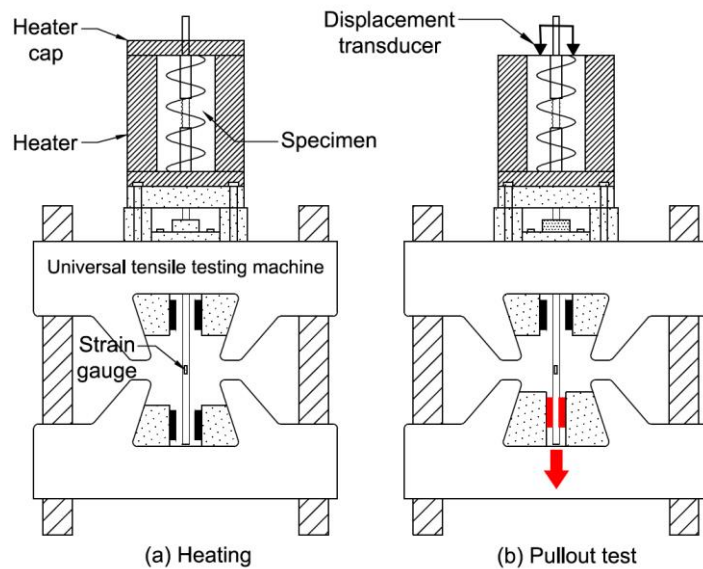


Fig. 7 Experiment phases

The temperature-time curves of the heater and the bond thermocouple are shown in **Fig. 8**. For the pull-out test (**Fig. 7b**), the heater cap on the top was removed and two displacement transducers, supported by the rebar top free end, were mounted on the top face of the concrete cylinder. Gripping the bottom extension, the tensile machine started the rebar pullout phase. To prevent any loading shock to the specimen and to provide constant loading

rate, according to JCI pullout test recommendations¹², tensile stress rate of 49.0 N/mm² per minute was subjected to the bar, i.e, 14kN/min (49.0N/mm²×286.5mm²=14.0kN). At elevated temperatures both steel yielding stress and bond strength reduce. To estimate the temperature in which the bar may yield before bond strength was reached, the BS8110 model was employed. Based on this model the bar might yield at 600°C before the bond strength was reached.

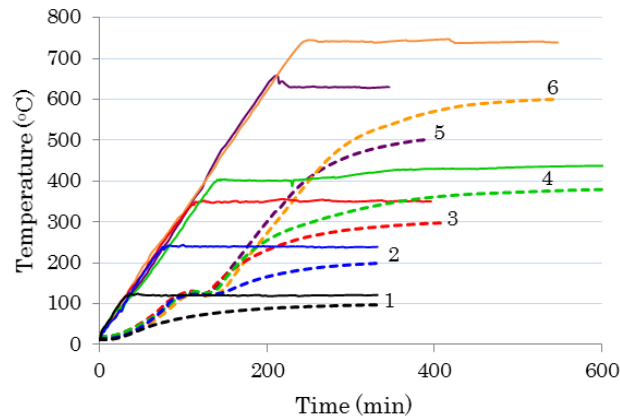


Fig. 8 Heat cycles (broken line: temperature in bond region, solid line: heater temperature)

RESULTS & DISCUSSION

IDELAZATION OF FIB BOND STRESS-SLIP RELATIONSHIP (TEST SERIES I)

The bond-slip relationships of test series I are shown in **Fig. 9** and the details of the results are summarized in **Table 4**.

Table 4 Bond strength and slip at each heat cycle

Temp. (°C)	Bond strength (MPa)				Residual bond strength	Slip at bond strength (mm)			
	(1)	(2)	(3)	Ave		(1)	(2)	(3)	Ave
20	12.0	13.1	12.1	12.4	1.00	0.65	0.82	0.99	0.82
100	10.0	9.6	9.7	9.8	0.79	0.62	0.66	0.64	0.64

200	11.7 ^{*1}	12.3	10.6	11.5	0.93	1.14 ^{*1}	0.59	0.82	0.85
300	12.0	10.4	9.1	10.5	0.90	0.82	0.57	0.88	0.70
400	9.2 ^{*2}	7.7 ^{*2}	7.3	8.1	0.74	1.15 ^{*2}	1.04 ^{*2}	1.06	1.15
500	6.4	6.5	6.4	6.5	0.52	1.01	0.94	0.86	0.97
600	6.2	5.5	4.9	5.5	0.47	1.01	0.93	1.36	0.97

*1 Test temperature= 170°C *2 Test temperature= 479°C

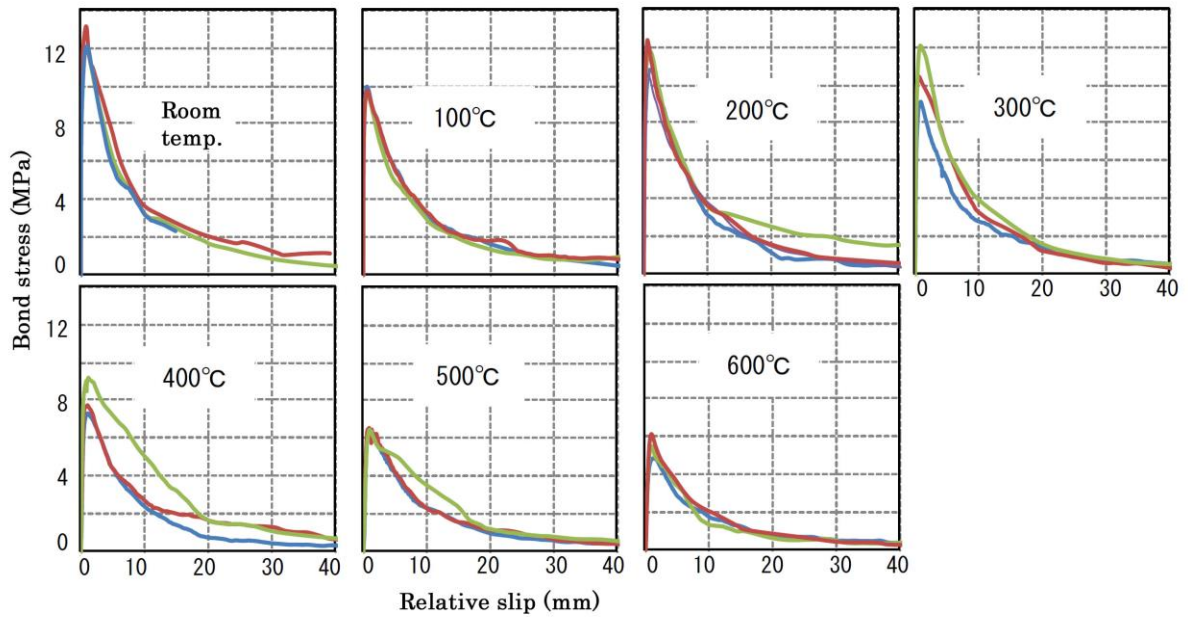


Fig. 9 Bond stress-slip relationship (Series I: $f_c=24\text{MPa}$)

According to *fib* Model (**Table 1**), the test specimens can be categorized as confined concrete with good bond condition; therefore, τ_{\max} and τ_f are 12.2MPa and 4.9MPa, respectively. **Fig. 10** shows the bond-slip relationship of the test specimens at room temperature based on *fib* Model. As can be seen in the figures, the ascending branch of the model lies within the test results. However, there is a large difference between the test results and other branches of *fib* Model. Some researchers (Harajli et al. 2004; Huang et al. 1996) have modified the *fib* Model by adding a straight line that reaches 0 at a certain slip. In this paper only the ascending branch of *fib* Model (**Eq. 4**) was focused for the test specimens at high temperatures.

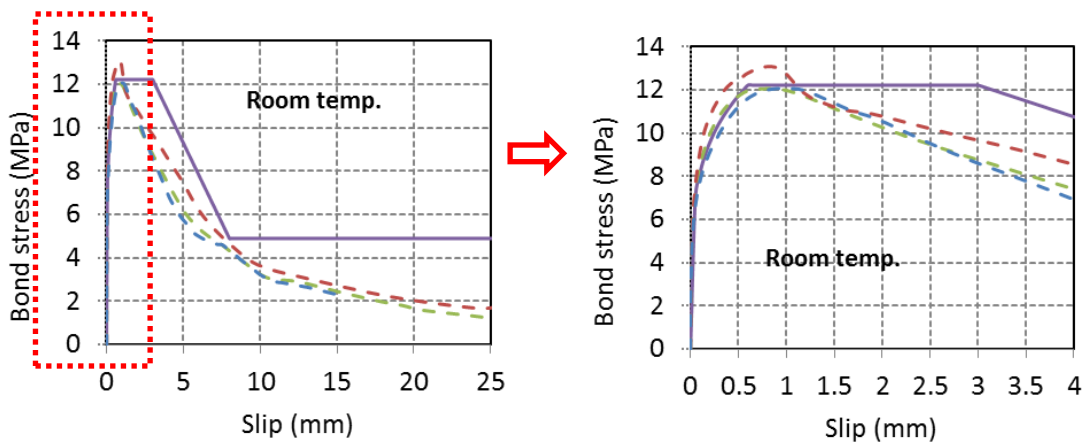


Fig. 10 fib Model vs test curves at room temp.

Regarding to slip (s_1) corresponding to bond strength, no linear correlation was found in the test data, hence the recommended value of *fib* Model for the test conditions is set as an insensitive parameter to temperature in the whole formulations. To idealize the ascending branch of *fib* Model at higher temperatures, a reduction factor ($k_{\tau,T}$) is multiplied on the maximum bond stress given by the model:

$$\tau_{\max} = k_{\tau,T} \cdot 2.5(f'_c)^{1/2} \quad \text{Eq. (8)}$$

Two different reduction factors were employed to be substituted in **Eq. 8**: (1) AIJ (Architectural Institute of Japan) concrete strength reduction factor¹⁴ (Model A), and (2) bond strength reduction factor at elevated temperatures recommended by Z. Huang¹⁰ based on Bazant and Kaplan bond stress-temperature curves (Model B). The reduction factor in Model B is defined as below:

$$k_{\tau,T} = 1.0 - \frac{0.22}{360}(T - 20) \quad 20 \leq T \leq 380 \text{ }^\circ\text{C} \quad \text{Eq. (9)}$$

$$k_{\tau,T} = 0.78 - \frac{0.75}{270}(T - 380) \quad 380 \leq T \leq 650 \text{ }^\circ\text{C} \quad \text{Eq. (10)}$$

$$k_{\tau,T} = 0.03 \quad T \geq 650 \text{ }^\circ\text{C} \quad \text{Eq. (11)}$$

Applying the two models to **Eq. 8** results in two different curves. **Fig. 11** shows the residual bond strength curves based on the two reduction models. Except at 100 °C, Model B seems to give more accurate results. However, this model predicts conservative values for temperatures beyond 500 °C. For the purpose of this section, Model B was employed. Regarding to the parameter α , the following equation was found to best fit at temperatures above 100°C for the test:

$$\alpha(T)=0.0012T+0.2$$

Eq. (12)

Fig. 12 shows the modified *fib* Model at high temperatures with the test results. As can be seen in the figures, at 100 °C and 600 °C the implemented formulations predicted higher and lower bond strengths, respectively. As the temperature rises the initial rising slope of the curves decrease and since the introduced model works based on exponential behavior of **Eq. 4**, it may not match the initial values (low bond-stress) of the tests. The proposed model is not expected to fit well with other experimental works with different test conditions. The more empirical data is accumulated, the better fit models will be proposed.

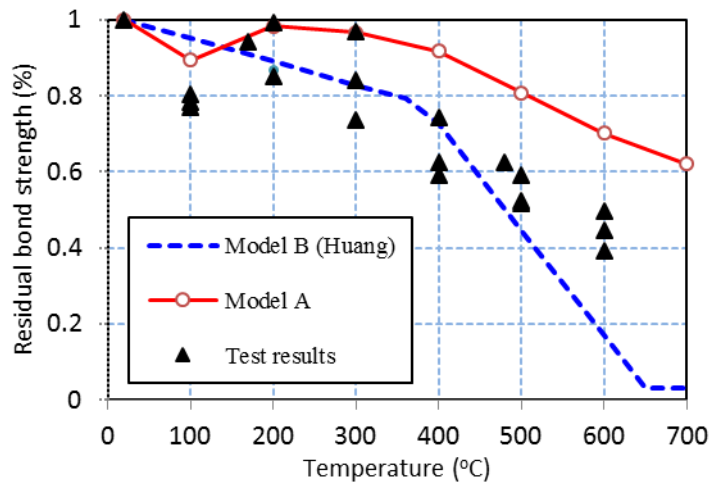


Fig. 11 Comparison of residual bond strength between test results and Models A and B

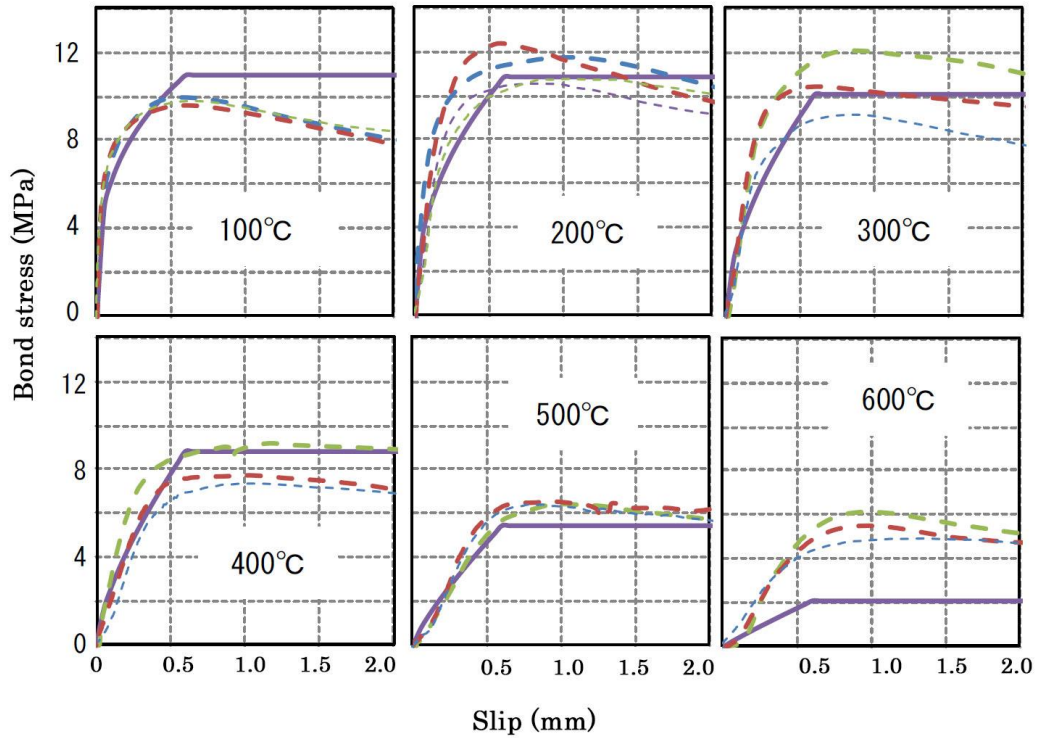


Fig.12 Modified *fib* Model (solid lines = modified *fib* model curves)

INFLUENCE OF CONCRETE STRENGTH ON BOND & SLIP (SERIES II)

In the second part, based on the test results of the two test series, the bond characteristics such as bond-slip relationships, and initial bond stiffness at elevated temperatures are discussed.

Bond stress-slip relationships at elevated temperatures

Fig. 13 shows the bond-slip curves of the test series II and **Fig. 14** shows the mean curves for the slip range of 0 to 0.5mm. As can be seen in the figures, as the temperature rises the bond strength decreases. This is mainly attributed to the loss of compressive strength of the concrete, however, the influence of steel stiffness and yield stress degradation should be appreciated as well. **Fig. 15** draws a comparison between the two series' bond strengths. As can be seen in the figure, the specimens of Series II, which benefited from larger concrete compressive strength (36.9MPa) developed approximately 20% larger bond strengths than those of Series I.

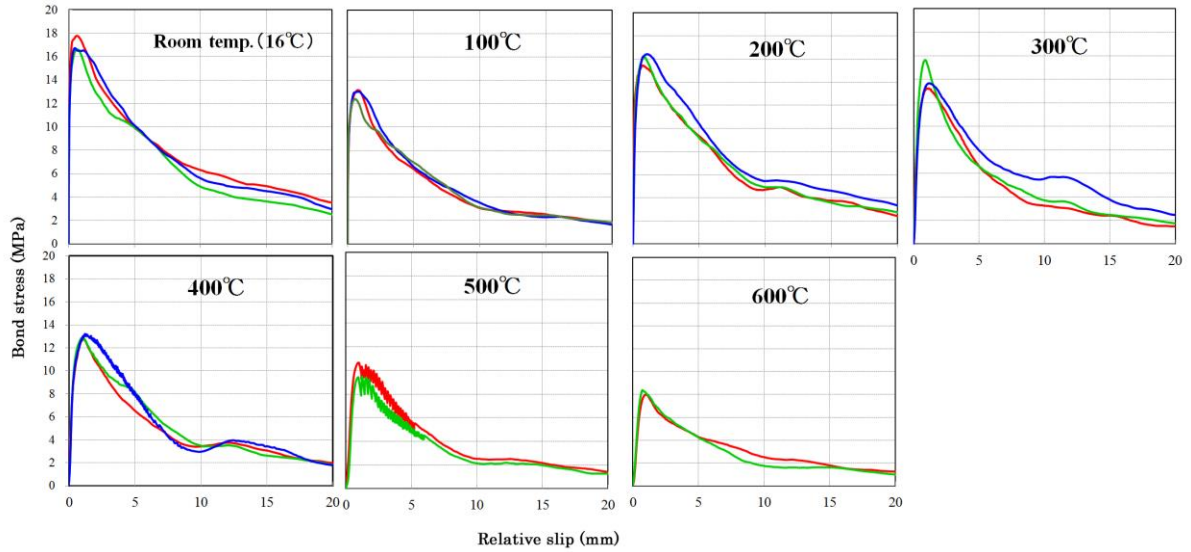


Fig. 13 Bond stress-slip relationships of test series II

In the **Fig. 15** a sudden loss in the bond strengths of the two series at 100 °C is apparent, which is very similar to the concrete compressive strength reduction trend. This apparent loss which is largely reversible at 200 °C is attributed to the weakening of the physical Van der Waal’s forces as the expanding water molecules push the CSH (Calcium Silicate Hydrate) layers further apart¹⁵. Upon this temperature up to 200 °C, the evaporated free water contributes to the cement hydration and the concrete recovers its compressive strength as high as 95% of the original one. Upon 200 °C, the decreasing trend continues, especially between 400 °C to 600 °C the large decrease is considerable and attributed to the decomposition of Portland cement components at the mentioned heat range¹⁵.

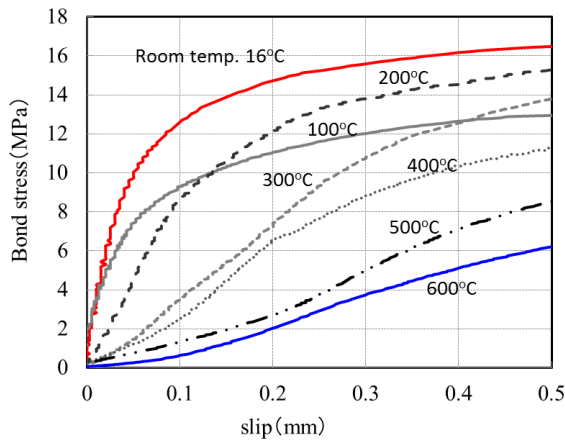


Fig. 14 Bond-slip relationship comparison

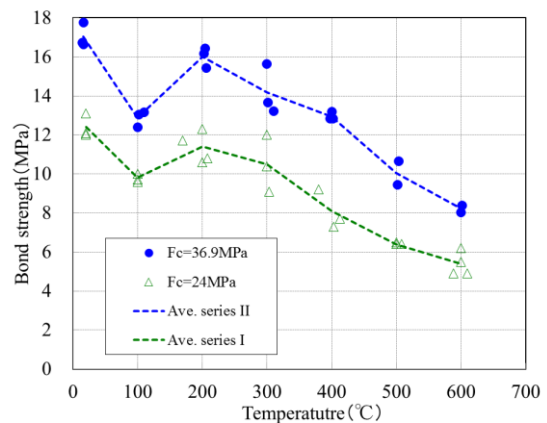


Fig. 15 Average bond strength

Fig. 16 shows the average residual bond strengths of the two series. In the figure, the bond stress reduction (model by Z. Huang) and AIJ concrete strength reduction (Model A) are plotted as well. As can be seen in the figure, the difference between the residual bond strengths of the two series up to 300°C are relatively small. However, in higher temperatures the specimens in series I sustained lower residual strength values. Here again the similarity between the decreasing trends of the residual bond strength and the concrete compressive strength is remarkable.

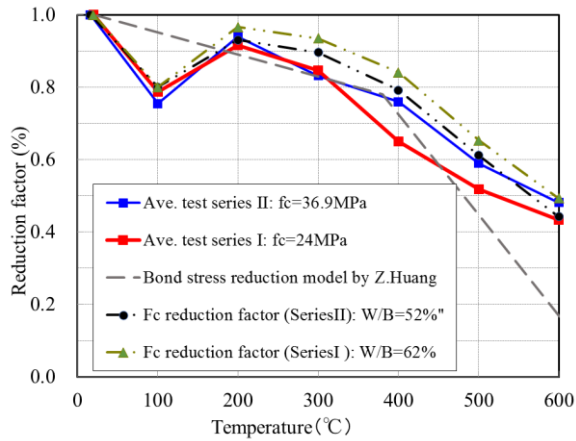


Fig. 16 Residual bond strength plotted against temperature

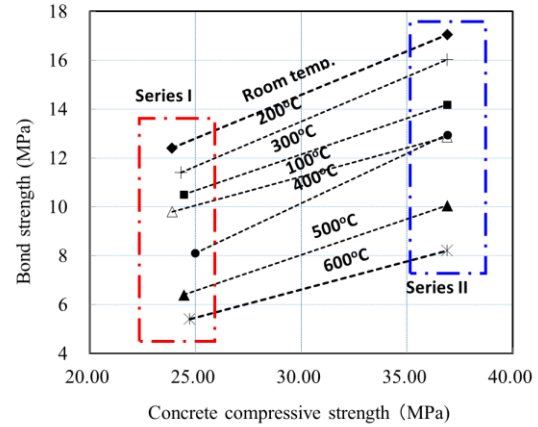


Fig. 17 Influence of concrete strength on bond strength

As it was mentioned earlier, according to BS8110 reduction model, the steel was likely to yield at 600°C. If the bar yields then the extent of contribution of concrete and steel strengths degradation in bond mechanism should be taken into consideration; however, to date a few studies have been done about this issue. **Fig. 17** draws a comparison of bond strength between the two series of tests. As it is plotted in the figure, the larger the compressive strength of the concrete is, the higher the bond stress is developed.

Slip at bond strength

Fig. 18 and **19** show the ratio of slip at the bond strength and the influence of concrete compressive strength on the slip at the bond strength, respectively. The discrepancy of slip values at the corresponding bond strengths was relatively large. As can be seen in the figures, the range of slip at bond strength fluctuated between 0.71 to 1.10mm in average.

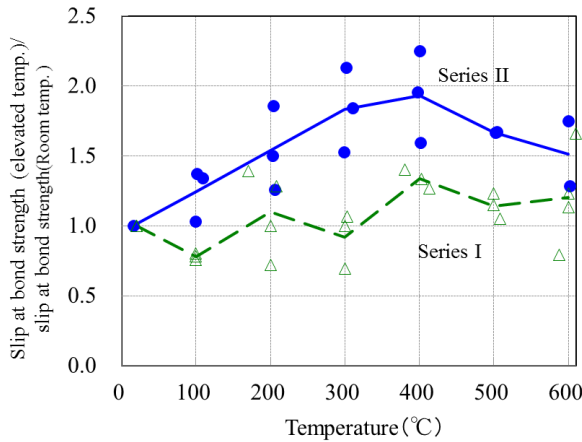


Fig. 18 Slip at bond strength

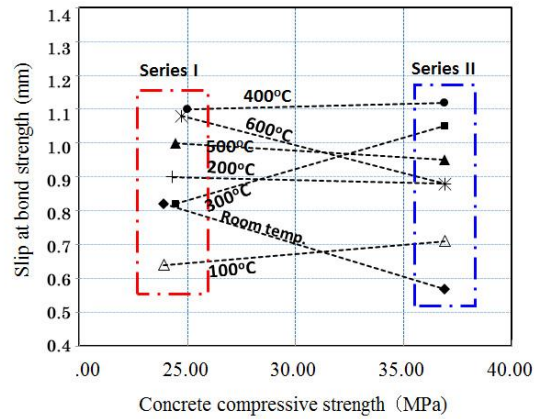


Fig. 19 Influence of concrete strength on slip at bond strength

Bond stiffness

The bond-slip curves of the specimens (**Fig. 14**) can be separated mainly into two groups; (1) up to 100 °C, the bond stresses are developed with an initial steep slope (almost 90 degrees) starting from a certain low bond stress and exponentially grows until it peaks at the bond strength, and (2) beyond 100 °C, the curves are developed with very gradual slope from the origin and peaking at the bond strength. **Fig. 20** shows two bond-slip curves of the test and the corresponding initial slopes (red lines). The authors defined the initial stiffness based on RC member subjected to service loads, in which the developed stresses in concrete is limited to one-third of concrete compressive strength. Hence, the initial bond stiffness could be defined as **Eq.12** and **13**:

$$K(T) = \frac{\frac{1}{3}\tau_{max}(T) - \tau_{s=0}(T)}{S_{\frac{1}{3}\tau_{max}(T)}} \quad T \leq 100^{\circ}\text{C} \quad \text{Eq. 12}$$

$$K(T) = \frac{\frac{1}{3}\tau_{max}(T) - \frac{1}{6}\tau_{max}(T)}{S_{\frac{1}{3}\tau_{max}(T)} - S_{\frac{1}{6}\tau_{max}(T)}} \quad T > 100^{\circ}\text{C} \quad \text{Eq. 13}$$

where, $K(T)$ is the initial bond stiffness, and τ_{max} is the bond strength. **Fig. 21** shows the initial bond stiffness of the two test series. Due to the scattered values of the initial bond

stiffness, the extent of influence of concrete compressive strength on the initial bond stiffness was not clearly understood. The reduction factor of the initial bond strength is illustrated in **Fig. 22**. As it is shown in the figure, beyond 300 °C regardless of concrete strength, the initial bond stiffness decreases remarkably to approximately as low as 20%. **Fig. 23** shows the influence of concrete compressive strength on the initial bond stiffness. **Table 4** shows the details of bond characteristics of the specimens of Series II.

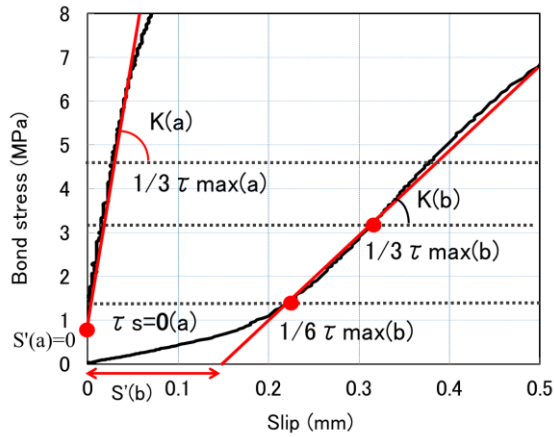


Fig. 20 Definition of initial bond stiffness

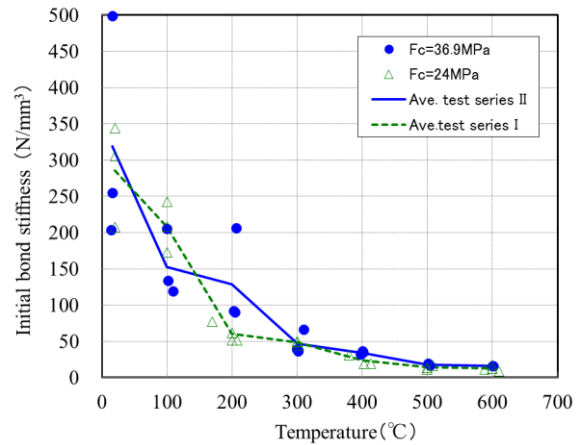


Fig. 21 Initial bond stiffness vs. temperature

Specimens before and after the tests

Fig. 24 (a) and **(b)** show the bond zone after the pullout test at room temperature, and at 600°C, respectively. The pictures were taken several months later. As can be seen in the figures, there are distinct gaps between each of the two lugs, which imply the complete crushed matrix at those zones. However, the heated specimen apparently suffered severe losses of concrete and steel mechanical properties. Thermal induced cracks are seen in **Fig. 24 (b)**.

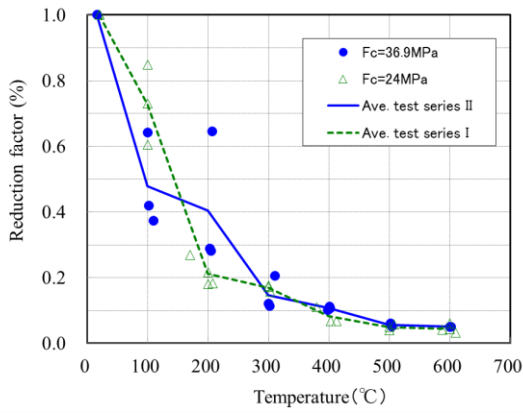


Fig. 22 Reduction factors for initial bond stiffness at elevated temperatures

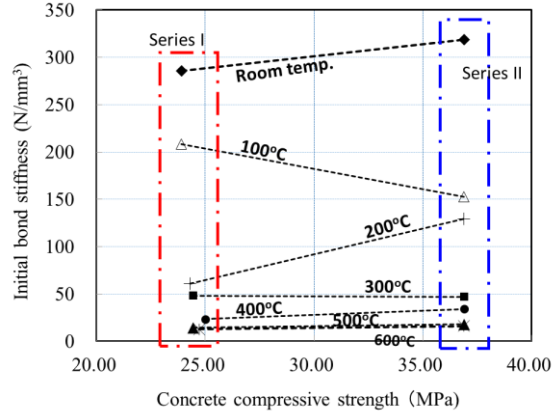
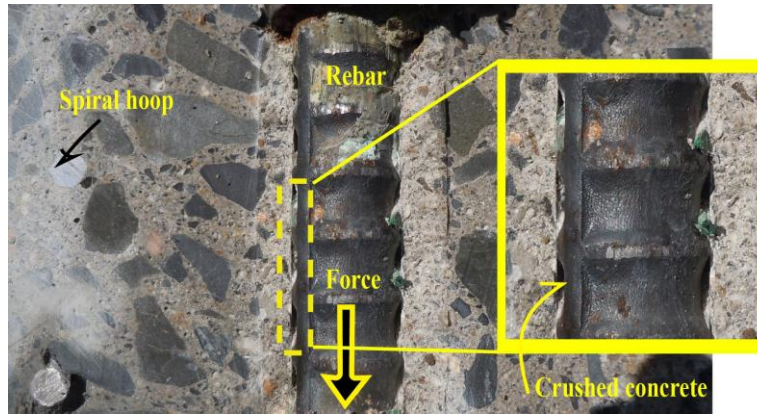
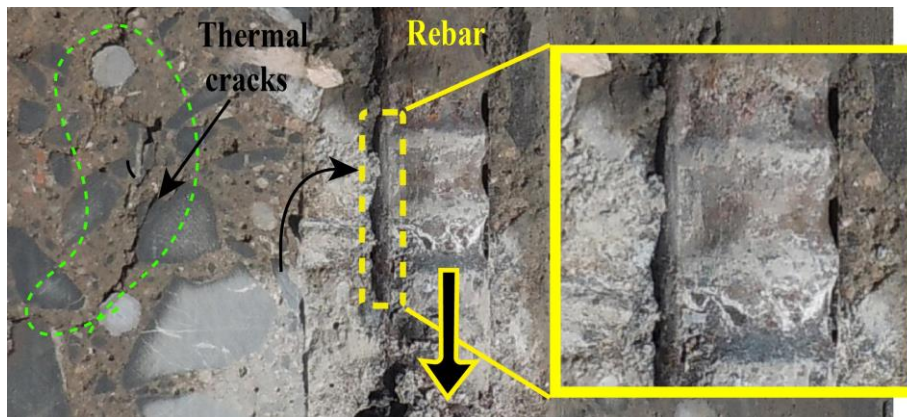


Fig. 23 Influence of concrete strength on initial bond stiffness



(a) Room temperature



(b) 600°C

Fig. 24 Bond condition after the test

Table 5 Bond mechanical characteristics of series II

Temperature (°C)		Initial bond stiffness (N/mm ³)	Ave. (N/mm ³)	Ratio	S'(T) (mm)	Ave. (mm)	Bond strength (MPa)	Ave. (MPa)	Ratio	Slip at bond strength (mm)	Ave. (mm)	Ratio (%)
Target	Actual											
Room temp.	16.5	498.82	318.9	1.00	0.00	0.00	17.78	17.05	1.00	0.60	0.57	1.00
	16.8	254.32					16.64			0.65		
	14.5	203.54					16.73			0.46		
100°C	109.8	119.23	152.54	0.37	0.00	0.00	13.17	12.87	0.77	0.77	0.71	1.34
	101.9	133.64		0.42			13.04		0.76	0.78		1.37
	99.8	204.77		0.64			12.40		0.73	0.59		1.03
200°C	206.6	205.93	129.15	0.65	0.007	0.008	15.44	16.02	0.91	0.72	0.88	1.26
	202.9	91.82		0.29	0.004		16.18		0.95	0.86		1.50
	204.5	89.70		0.28	0.012		16.43		0.96	1.06		1.85
300°C	310.6	65.77	46.84	0.21	0.025	0.026	13.23	14.18	0.78	1.05	1.05	1.84
	299.6	38.63		0.12	0.015		15.64		0.92	0.87		1.53
	301.7	36.14		0.11	0.040		13.66		0.80	1.22		2.13
400°C	397.7	32.21	34.12	0.10	0.014	0.027	12.83	12.95	0.75	1.12	1.10	1.95
	402.1	34.26		0.11	0.032		12.83		0.75	0.91		1.59
	400.7	35.89		0.11	0.036		13.20		0.77	1.29		2.25
500°C	504.1	16.53	17.88	0.05	0.041	0.096	10.66	10.05	0.63	0.96	0.95	1.67
	502.0	19.24		0.06	0.151		9.44		0.55	0.95		1.67
600°C	600.4	16.17	16.03	0.05	0.077	0.057	8.02	8.21	0.47	1.00	0.88	1.75
	601.9	15.90		0.05	0.037		8.39		0.49	0.73		1.28

CONCLUSIONS

In this work two series of pullout tests at elevated temperatures have been conducted. With respect to the objectives of this research the following conclusions can be drawn;

1. Based on the equation of the ascending branch of *fib* Code Model (2010) for bond-slip relationship, a series of temperature-dependent formulations has been introduced. The generated results of the proposed model up to 500 °C lie within the test results. However, the model predicted relatively higher bond stress values at 100°C since it does not consider the sharp concrete strength loss at 100 °C. The model is expected to work well for other similar experiments, however, the verification of the model needs more empirical data.
2. The initial bond stiffness decreased as the temperature increased. Especially beyond 300°C a considerable loss in the initial bond stiffness led to the change in the curve of the bond-slip relationships. In other words, the introduced model may not be able to predict the slip at very low bond-stresses at elevated temperatures.
3. An apparent decrease in the bond strength of the specimens occurred at 100 °C that was largely reversible at 200 °C. This sudden sharp loss may be attributed to the loss of concrete compressive strength due to the weakening of the physical Van der Waal's forces when the expanding water molecules push the CSH (Calcium Silicate Hydrate) layers further apart.
4. Series II showed approximately 20% larger bond strengths in average. However, as for initial bond stiffness, especially at temperatures beyond 300°C, no considerable difference was observed.
5. The current study work provided a series of reduction factors compatible to the test conditions. The models are currently being inserted into related FE models to get checked and regulated for the future numerical studies.

ACKNOWLEDGMENT

This research work was financially supported by JSPS KAKENHI Grant Number 23246101. Special thanks goes to Mr. Lim, Ota, Watanabe, and Ms. Tominaga for their great participation in this study work.

REFERENCES

1. Nishiyama. M, Lim. S, “Fire-Resistance Tests on statically indeterminate Reinforced Concrete Frame”, *AIJ*, 2011, pp 25-26 (in Japanese).
2. Raouffard. M, Sakashita. M, Nishiyama. M, “External reinforced concrete beam-column subassemblages in fire”, NZSEE, Auckland, Mar. 2013
3. Rehm, G. “Über die Grundlagen des Verbundes zwischen Stahl und Beton”, Heft 138, Deutscher Ausschuss für Stahlbeton. Verlag Wilhelm Ernst & Sohn, Berlin. 1961
4. Martin, H. “Zusammenhang zwischen Oberflächenbeschaffenheit, Verbund und Sprengwirkung bei Rippenstählen unter Kurzzeitbelastung”, Heft 228, DAfSTB. Verlag Wilhelm Ernst & Sohn, Berlin. 1973
5. Harajli, M. H. (2006). “Effect of confinement using steel, FRC, or FRP on the bond stress-slip response of steel bars under cyclic loading.” *Mater. Struct.* , 39 , 621–634
6. Wu, Y. and Zhao, X. . “Unified Bond Stress–Slip Model for Reinforced Concrete.” *J. Struct. Eng.*, 139(11), 1951–1962.
7. “Bond of reinforcement in concrete”, Bulletin 10, ISBN 978-2-88394-050-5, August 2000, www.fib.international.org
8. “*fib* Model Code for concrete structures 2010”, vols. 1&2, final draft, vols. 1&2, final draft, Bulletin 55
9. Bazant, Z.P. and Kaplan, M.F., “Concrete at High Temperatures”, Longman Group Limited, 1996.
10. Huang, Z. "Modelling the bond between concrete and reinforcing steel in a fire." *Engineering Structures*, 32(11), 3660-3669.
11. Hiroshi Matsuyoshi : Study on fire-resistance of FRP retrofitted RC structure, *Journal of Concrete Engineering* , Vol. 25, pp.329-334, 2005 (Japanese)
12. Murata J. : “Method of test for bond strength between concrete and reinforcing steel bar” *Concrete Journal*, Vol. 18, No.4 pp.14~22, April 1980 (Japanese)
13. Ichise K., “Mechanical properties of high strength concrete at high temperatures” *Concrete Journal*, Vol. 21, No.2, pp.1105~1110, April 1999 (Japanese)
14. Architectural institute of Japan “Guidebook for fire-resistive performance of structural materials” pp. 40-54, 2009
15. “Fire design of concrete structures - materials, structures and modelling”, Bulletin 38, ISBN 978-2-88394-078-9, Apr. 2007, www.fib.international.org